Control Stability of Inverters with Series-compensated Transmission Line: Analysis and Improvement

Qianjin Zhang[1]*, Jinhui Qian[1], Zhaorong Zhai[1], Mohammad Abusara[2], Xiaodong Liu[1], Sucheng Liu[1], Wei Fang[1], Hongbo Liu[3]

[1] School of Electrical and Information Engineering, Anhui University of Technology, Ma'anshan, CO 243000, Anhui, China

[2] Renewable Energy, the University of Exeter, Penryn, CO TR10 9EZ, Cornwall, UK.

[3] Qingdao Power Supply Company, Shandong Electric Power Company of State Grid, Qingdao, CO 266001, Shandong, China.

*Zqj1214@ahut.edu.cn

Abstract:

With the rapid development of renewable energy, large amount of power need to be transmitted to loads centers and series-capacitor compensation (SCC) plays an important role in the renewable power transmission. However, it has been pointed out that SCC interacts with inverters and threatens system stability. This research investigates the influence of SCC on inverters control and proposes the strategies for enhancing system stability based on the instability mechanism. The impact of SCC on inverter current control and synchronization control is firstly analyzed. The current control model is established by system transfer function and the synchronization control model focusing on transient stability is established based on the traditional synchronous reference frame phase-locked loop (SRF-PLL). The bode and nonlinear analysis methods are respectively utilized in stability analysis of the current and synchronization control. It is found that SCC has little effect on inverter current control but affects synchronization control seriously. SCC reduces the stability range of synchronization control and causes system instability when there is a large frequency disturbance. In order to improve system stability, two approaches of optimizing the PI controller and designing a band-pass filter (BPF) inside PLL are then proposed. Finally, the simulations and experiments are presented to verify the correctness of theories.

Keywords: Inverters, Grid integration, Reactive power compensation, Stability

1. Introduction

Renewable energy as a primary source of future energy has exploded in popularity in recent years [1]. In general, renewable energy such as wind or solar is difficult to connect directly to the power system. Inverters are the crucial component to realize energy conversion and grid integration. However, although inverters are very important, their control stability is always affected by the power grid [2]-[6].

In modern power systems that with substantial renewable energy penetration, grid following and grid forming are two basic types of grid-connected inverters [7,8]. Grid forming inverters are frequently used in microgrids that operate in island mode, supplying power to local loads without high-voltage long-distance transmission lines to transport power. Grid following inverters, on the other hand, are frequently used in big centralized renewable power plants for transmitting maximum power to the power grid. Because of the large distance between centralized renewable power sources and loads centers, grid following inverters generally work with the series-compensated transmission lines. As a result, this paper focuses on the effects of SCC on grid following inverters.

The stability of grid following inverters is mostly influenced by the weak power grid [9,10]. The transfer function based impedance model and differential equations based state space model are developed to study the stability problem [11-14]. The impedance-based method has a significant advantage when system detailed parameters are unknown because the impedance can be obtained by terminal measurements. However, the disadvantage is that it is difficult to identify the root-cause of the instability [15]. On the contrary, specific system parameters are normally required to create a state space model. The weakly damped and unstable modes of the system are able to be easily obtained, but the model order is quite large, necessitating an order reduction technique [16]. Despite the fact that these two common methods for evaluating system stability are the most popular, they are both based on small signal linearization technique, which makes it difficult to explain system dynamics under significant disturbances. Nonlinear stability analysis methods such as Lyapunov function and phase

This work was supported by the Youth Foundation of Anhui University of Technology under grant QZ202106 and the Natural Science Foundation of Colleges and Universities of Anhui Province under grant KJ2020A0246.

portraits are used to investigate the large signal characteristics, especially for PLL based synchronization control, where system stability is classified into static and dynamic stability problems [17-20].

Based on the stability analysis method, it is found out that inverter current control and synchronization control are prone to instability when gird impedance is considerable [21,22]. However, in most studies, the grid impedance is assumed to be inductive and SCC is not taken into account. In fact, in wind farms, SCC has been reported to interact with inverter control in doubly fed induction generators (DFIG) and cause sub-synchronous control interaction (SSCI) problems [22]-[26]. Even if the structure of the inverter is fundamentally different from DFIG, the system with SCC appears inferior stability performance than the system without SCC for general grid following inverters. To the authors' knowledge, few research has been done on the thorough stability analysis for the inverters system with SCC from the perspective of inverter's detailed control loops. Given that SCC is critical for the transmission of renewable energy and that its impact on inverter control has an influence on the overall system stability, more research needs to be done to look into the behind stability problems.

This paper aims to give a thorough analysis of the influence of SCC on inverter control. Firstly, the impact of SCC on inverter current control and synchronization control is analyzed, which is one main contribution of this paper. Then, the related stability enhancement approaches are proposed according to the instability mechanism, which is another contribution of this paper. Finally, simulations and experiments are used to verify the theory. The findings of this paper can provide reference for the investigation and resolution of inverter system instability problem caused by SCC, which contributes to the stable and reliable operation of gird-connected renewable power system.

The rest of this paper is organized as follows. Section 2 analyzes the influence of SCC on inverter control. Section 3 proposes the related stability improvement solutions according to the instability mechanism. Section 4 presents the simulation and experimental results to support the theories, followed by the conclusion in Section 5.

2. Stability analysis of inverters with SCC lines

SCC is required in long distance power transmission lines, but it also has an impact on inverter control stability. This section first analyzes the influence of SCC on inverter current control, and then goes into depth about the synchronization control.

Series compensation as one important compensation approach plays a vital role in reactive power compensation, especially for the situation that parallel compensation is ineffective. The simplified one-line diagram of inverter system with SCC is shown in Fig. 1. where L_1, C, L_2 are inverter's LCL filter and L_g, C_g are the corresponding grid inductor and series compensation capacitor. Parameter n denotes the paralleled number of inverters. The main parameters of a typically used 500 kW inverter in large PV plants are provided in Table I in Appendix.

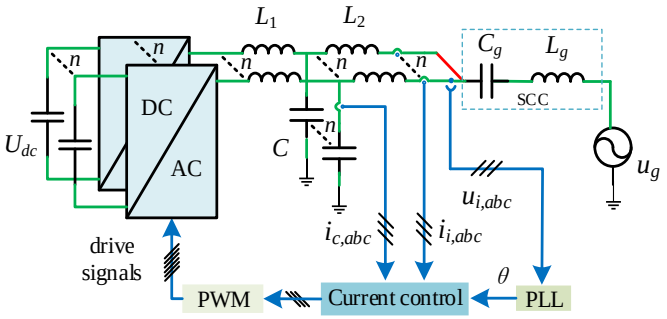

Fig. 1. Simplified one-line diagram of a three-phase grid-connected inverter system with SCC.

Given that this paper focuses on the impact of SCC on inverter control, the interaction between inverters is ignored. The system can be equivalent to a single inverter system [7], [27]. The grid impedance and series capacitor are correspondingly as:

$$Z_g(s) = nsL_g + \frac{n}{sC_g}. \tag{1}$$

The amplitude of $Z_g(s)$ can be calculated by:

$$\left|Z_g\right| = n\left|\omega L_g - \frac{1}{\omega C_g}\right| \tag{2}$$

where ω is system angular frequency. Equation (2) shows that SCC works directly on the grid inductor to minimize the total grid impedance. And ideally, the amplitude of grid impedance can be compensated to zero when $\omega L_g=1/\omega C_g$. In general, ω is assumed as the constant grid frequency ω_g and SCC is designed when $\omega=\omega_g$. However, in an inverter system, the frequency is determined by inverter synchronization control and often deviates from ω_g during system dynamic process. Therefore, $Z_g(s)$ shows great fluctuation in response to the change of inverter control, and is easy to affect inverter control.

2.1 SCC's effect on inverter current control

Fig. 2 depicts the diagram of inverter current control taking into consideration of SCC, where $G_c(s)$ is the PR controller and k_c is the active damping coefficient realized via capacitor current feedback. $Y(s)$ is the inverse of grid impedance ($Z_g(s)$).

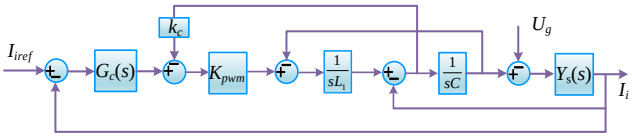

Fig. 2. Diagram of inverter current control loop considering SCC.

According to Fig. 2, the open-loop transfer function of the current control loop is derived as:

$$T_s(s) = \frac{Y_s(s)G_c(s)K_{pwm}}{s^2L_1C + sCk_cK_{pwm} + Y_s(s)sL_1 + 1} \tag{3}$$

where

$$\begin{cases} G_c(s) = k_p + \dfrac{2k_r\omega_c s}{s^2 + 2\omega_c s + \omega_0^2} \\ Y_s(s) = \dfrac{sC_g}{s^2 C_g (L_2 + nL_g) + 1} \end{cases} . \quad (4)$$

The Bode diagram of (3) is shown in Fig. 3. The instance without SCC is shown by the red-dotted line. The green-solid and blue-dash-dotted lines represent the conditions that system short circuit ratio (SCR) is lowered (i.e. SCC increased). It has been discovered that decreasing SCR causes a decrease in system phase margin. This behavior is consistent with the system without SCC [21]. Therefore, the series capacitor has minimal effect on inverter current control. This is further demonstrated by the impedance spectrum of Z_g (s) which shows that the amplitude and phase are almost identical regardless of whether SCC is employed in the frequency range that current control works.

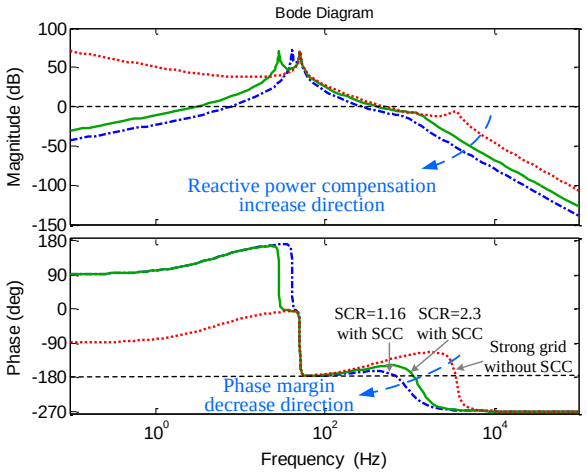

Fig. 3. Bode diagram of inverter inner current control loop

2.2 SCC's effect on inverter synchronization control

In Fig. 1, the input signal of the PLL is the inverter output voltage which is directly regulated by SCC. Therefore, SCC is incorporated into PLL's control by inverter output voltage.

According to the current control diagram in Fig. 2, inverter can be modeled as a Norton equivalent circuit from the power grid perspective [9]. And the current source is determined by inverter current reference and PLL. Take the PLL control into account, the entire system is depicted in Fig. 4, where $G_i(s)$ and $Y_i(s)$ are the transfer function from current reference and inverter output voltage to inverter output current that can be derived by Fig. 2, and:

$$G_i = \frac{K_{pwm}G_c}{L_1L_2Cs^3 + K_cK_{pwm}L_2Cs^2 + (L_1+L_2)s + K_{pwm}G_c} , \quad (5)$$

$$Y_i = \frac{L_1Cs^2 + K_cK_{pwm}Cs + 1}{L_1L_2Cs^3 + K_cK_{pwm}L_2Cs^2 + (L_1+L_2)s + K_{pwm}G_c} . \quad (6)$$

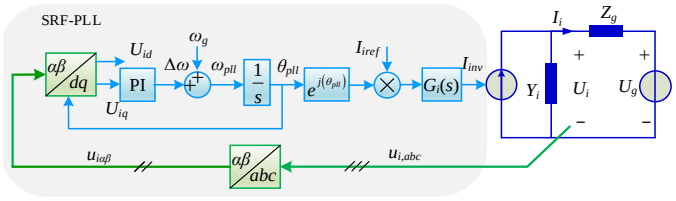

Fig. 4. Equivalent model of inverter synchronization control in grid-connected system.

As inverter output voltage U_i is the important part connecting PLL control and inverter circuit. The stability analysis model should be deduced start from U_i. Taking inverter current reference and grid voltage as the input variables, U_i is expressed as:

$$U_i = T_v(\omega_g)U_g + T_i(\omega_{pll})G_i(\omega_{pll})I_{iref} \quad (7)$$

where ω_g is grid frequency and ω_{pll} is inverter output current frequency:

$$T_v(\omega_g) = \frac{1}{1+Y_i(\omega_g)Z_g(\omega_g)}, \quad T_i(\omega_{pll}) = \frac{Z_g(\omega_{pll})}{1+Y_i(\omega_{pll})Z_g(\omega_{pll})} . \quad (8)$$

Expressing U_i in its exponential form [28]:

$$U_i = \left|T_v(\omega_g)U_g\right| e^{j(\theta_v+\theta_g)} + \left|T_i(\omega_{pll})G_i(\omega_{pll})I_{iref}\right| e^{j(\theta_i+\theta_{pll})} \quad (9)$$

where '| |' represents calculating amplitude, θ_v, θ_g, and θ_i are respectively the phases of T_v, U_g, and T_iG_i, and θ_{pll} is the phase outputted by PLL.

In dq frame, U_i is expressed as U_{idq} and,

$$\begin{aligned} U_{idq} &= U_i e^{-j\theta_{pll}} \\ &= \left|T_v(\omega_g)U_g\right| e^{j(\theta_v+\theta_g-\theta_{pll})} + \left|T_i(\omega_{pll})G_i(\omega_{pll})I_{iref}\right| e^{j\theta_i} \end{aligned} . \quad (10)$$

The component U_{iq} in q axis is used for phase-locked control, and is given by:

$$\begin{aligned} U_{iq} &= \left|T_v(\omega_g)U_g\right| \sin(\theta_v + \theta_g - \theta_{pll}) \\ &\quad + \left|T_i(\omega_{pll})G_i(\omega_{pll})I_{iref}\right| \sin(\theta_i) \\ &= V_v + V_i \end{aligned} . \quad (11)$$

Substituting (11) into Fig. 4, the simplified model is shown in Fig. 5, where V_v represents the grid voltage effect and V_i represents the inverter current impact. According to (11), V_v and V_i, are the functions of system frequency and are influenced by grid inductor, SCC and inverter current control loop. When system frequency is operating at fundamental frequency, according to (8) and (9), V_i is almost zero because of the existence of SCC. However, when system frequency has a large disturbance, V_i is considerable to interact with V_v to threaten system stability.

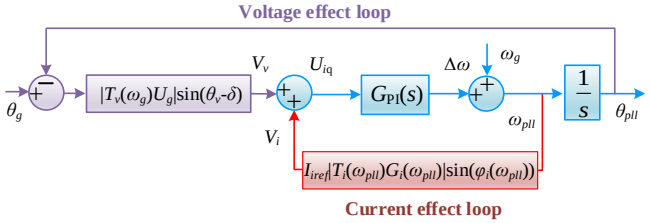

Fig. 5. Simplified model of inverter synchronization control

In order to further investigate the stability problem, system is equivalently transformed into its second-order differential form. According to Fig. 5, PLL's output signal θ_{pll} is expressed as [29]:

$$\begin{aligned}\theta_{pll} &= \int\left(\omega_0 + K_P U_{iq} + K_I \int U_{iq} dt\right) dt \\ &= \theta_g + \int\left(K_P U_{iq} + K_I \int U_{iq} dt\right) dt\end{aligned}. \tag{12}$$

Assuming θ_{pll}-θ_g=δ, after twice differential operations, it is simplified as:

$$\ddot{\delta} = K_P \dot{U}_{iq} + K_I U_{iq}. \tag{13}$$

Taking x_1=δ, x_2=$\dot{\delta}$, the original system is expressed as:

$$\begin{cases}\dot{x}_1 = x_2 \\ \dot{x}_2 = K_P \dot{U}_{iq} + K_I U_{iq} = f\left(x_1, x_2\right)\end{cases}. \tag{14}$$

According to (14), system phase portraits are plotted and shown in Fig.6. Comparing Fig.6(*a*) and Fig.6(*b*), it can be observed that when a substantial frequency variation occurs, system becomes unstable. This is due to the fact that SCC only acts on the fundamental frequency point, whereas the non-fundamental frequency points have a big V_i. As V_i is determined by SCC and inverter current reference, system stability should be improved when SCC and/or current reference are reduced. Fig.6(*c*) and Fig.6(*d*) prove that when SCC and current reference are lowered, the unstable system becomes stable again even with the same considerable frequency deviation.

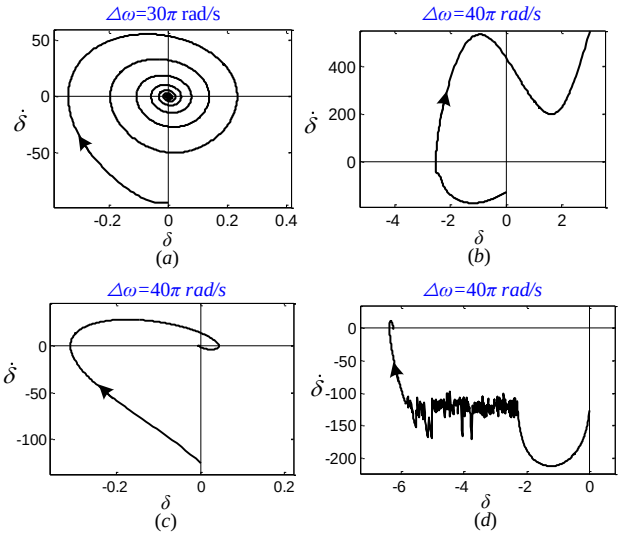

Fig. 6. System phase portraits. (*a*) small frequency deviation, (*b*) large frequency deviation, (*c*) small SCC (*d*) small I_{iref}

Actually, V_i can be viewed as a disturbance injected into system synchronization control by inverter current. The system can only be stable if V_v is able to counteract V_i and ensure U_{iq}=0. Therefore, V_i should be smaller than the maximum value of V_v [31], the inverter current reference should then satisfy:

$$I_{iref} \le \frac{\left|T_v\left(\omega_g\right)U_g\right|}{\left\|T_i\left(\omega_{pll}\right)G_i\left(\omega_{pll}\right)\right|\sin\left(\theta_i\right)}. \tag{15}$$

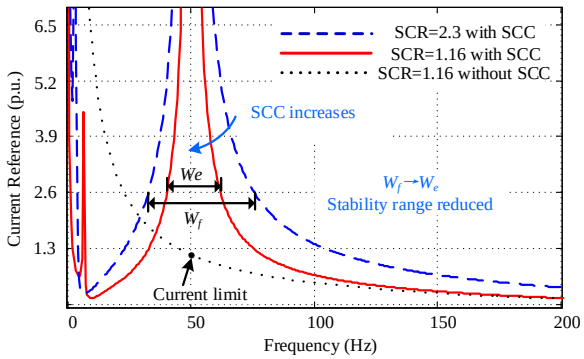

Fig. 7. Curves of the maximum current reference for system stability

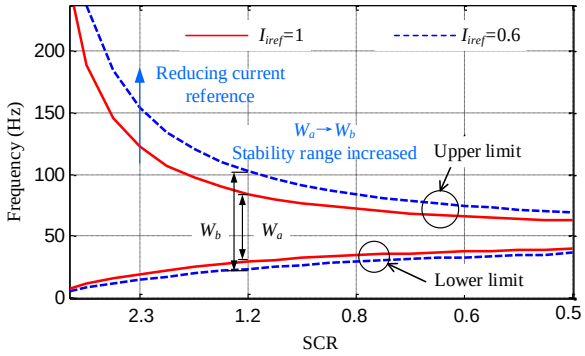

Fig. 8. Limitations of system frequency deviation under constant current reference

Equation (15) gives the maximum limit of inverter current reference for system stability throughout the whole frequency range. The maximum current reference versus frequency is plotted in Fig. 7 where the per unit value of current is given with the rated value of 1512 A (500 kW system). When the real current reference exceeds the curves, system control will lose its equilibrium point and become unstable. When the system frequency deviation is significant, the real current reference can easily exceed the curve limits for a given current reference. Accordingly, two conclusions can be drawn by Fig.7. (1) SCC deteriorates system stability in the frequency range below the fundamental frequency. This can be explained by the comparison of the system with and without SCC (red-solid and black-dotted lines in Fig. 7). The maximum current curves with SCC (red-solid line) are obviously below the curve without SCC (black-dotted line) in low frequency range. (2) For a given current reference, the increase of SCC reduces system stability range. This is concluded by the blue-dashed line and red-solid line where smaller SCR corresponds to bigger SCC. It shows that the increase of SCC reduces the range of frequency deviation that satisfies the current reference below the maximum curve. To be more intuitive, the allowable frequency deviation range for system stability under constant current reference is shown in Fig.8. It can be observed that when SCR is reduced, two curves progressively approach 50 Hz, indicating that a system with greater SCC allows for smaller frequency variation. Smaller current references, on the other hand, increase system stability in systems with a constant SCC. This

is because that reducing current reference effectively enlarges the permitted frequency deviation range according to the comparison between the red-solid line and blue-dashed line.

When system frequency deviation exceeds the stability range, V_i will be bigger than V_v. System frequency ω will deviate from ω_g and rise or fall under the action of PI controller until gets to a new equilibrium point where the dc component of U_{iq} is zero. The new equilibrium point ω_s can be predicted by V_i=0. This is because that V_v has no dc component but a sinusoidal signal oscillating at ω_g-ω:

$$V_v = \left|T_v\left(\omega_g\right)U_g\right|\sin\left(\left(\omega_g-\omega\right)t+\theta_v\right). \tag{16}$$

Due to U_{iq}=V_v+V_i, and V_v is unable to push ω moving, therefore, the new equilibrium point is determined by V_i. The plots of V_i are given in Fig. 9. The system with SCC are shown by the red solid line and the green dash-dotted line. Compared with the case without SCC (blue-dashed line), it can be observed that SCC leads to a large absolute value of V_i in the low frequency region, which accounts for the instability caused by SCC. On the other hand, by the comparison between the red-solid line and green-dash-dotted line, considering inverter current control loop reveals system another equilibrium point ω_s. Between 50 Hz and ω_s, the value of V_i is negative. When system frequency ω moves into this range, ω will keep decreasing until it reaches ω_s under the action of PI controller. When ω below ω_s, V_i becomes positive and makes ω increase. In the end, system frequency will be stable at ω_s. However, without taking into account the inverter current control loop, this equilibrium point and instability process are not visible. As a result, it can be stated that SCC influences system stability through its influence on V_i, and thus taking into account the inverter current control loop is critical in identifying system equilibrium points and instability process.

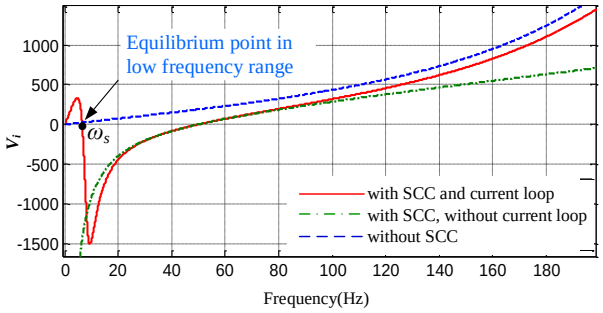

Fig. 9. Frequency scanning of V_i

To validate the theoretical analysis, the waveforms of system frequency under varied SCR and SCC are presented in Fig.10 using the model in Fig.5 and the parameters in Table I. The grid inductor and SCC are implemented at the time instant of 0.1 s. It is demonstrated in Fig.10(*a*) that the application of SCC results in frequency resonance for the same SCR system (by the comparison between the red-solid line and blue-dotted line), and aggravates the resonance range for smaller SCR system (by the comparison between the blue-dotted line and black-dashed line). When SCR is reduced further, SCC directly destabilizes the system as shown in Fig. 10(*b*) where system frequency deviates to another operation point ω_s and oscillates at ω_g-ω_s.

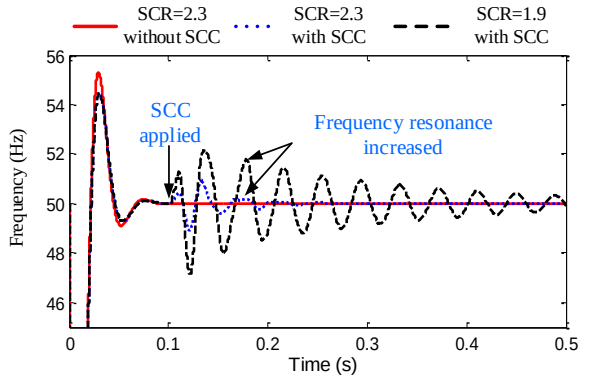

(*a*)

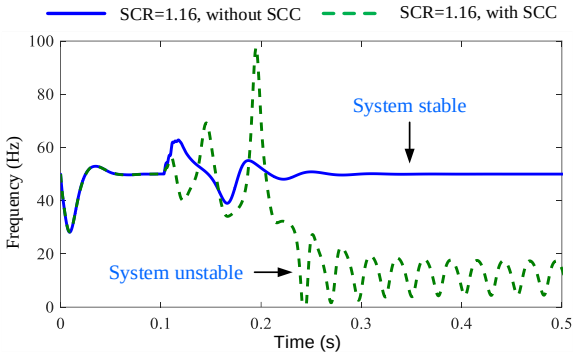

(*b*)

Fig. 10. Waveforms of PLL output frequency. (*a*): change of SCR and related SCC. (*b*): same SCR with and without SCC.

3. Stability improvement methods

As illustrated in section 2, the frequency deviation, inverter current reference, and SCC all have an impact on the stability of a system with SCC. However, the current reference and SCC are dictated by system capacity and operating circumstances that are difficult to adjust. Therefore, system stability can be enhanced by controlling frequency variation. Two solutions for controlling frequency deviation are given in this paper: changing the PI controller settings and constructing a BPF inde PLL.

The PI controller's transfer function is given by:

$$G_{PI}(s)=K_P+\frac{K_I}{s}. \tag{17}$$

According to Fig. 9, when system has a tiny frequency disturbance about 50 Hz, the current effect loop V_i is nearly zero, thus V_v is the major input signal to the PI controller at this moment, and the frequency deviation is able to be calculated by:

$$\begin{aligned}\Delta\omega &= K_P V_v + K_I\int V_v dt \\ &= K_P\left|T_v U_g\right|\sin\left(\Delta\omega t+\theta_v\right)-\frac{K_I\left|T_v U_g\right|}{\Delta\omega}\cos\left(\Delta\omega t+\theta_v\right)\end{aligned} \tag{18}$$

rearranging,

$$\Delta\omega = A_{ac}\sin\left(\Delta\omega t+\theta_v+\theta_{ac}\right) \tag{19}$$

where

$$\left.\begin{aligned} A_{ac} &= \left|T_v U_g\right| \sqrt{K_P^{\,2} + \left(\frac{K_I}{\Delta\omega}\right)^2} \\ \theta_{ac} &= \arctan\left(\frac{-K_I}{K_P \Delta\omega}\right) \end{aligned}\right\}. \tag{20}$$

Parameters K_P and K_I are related to the amplitude of $\Delta\omega$. Therefore, the frequency deviation is able to be reduced by reducing K_P and/or K_I.

In order to provide a reference for designing PI parameters to improve system stability, the cutoff frequency of PI controller is defined as ω_p, and:

$$\omega_P = \sqrt{\frac{2K_I^2}{1-2K_P^2}}\,. \tag{21}$$

According to (21), for a real cutoff frequency, K_P must be smaller than $1/\sqrt{2}$. Then, K_I is able to be calculated by a well-defined A_{ac} by substituting K_P into (20) based on a selected small $\Delta\omega$.

According to (20), smaller K_P and K_I can help to limit system frequency deviation, but it also increases system response time [32]. A tradeoff must be made when using a PI controller to avoid the instability induced by SCC.

In order to overcome the limitation of adjusting PI controller, the frequency deviation can be restricted by a band-pass filter outside of PI controller as shown in Fig. 11.

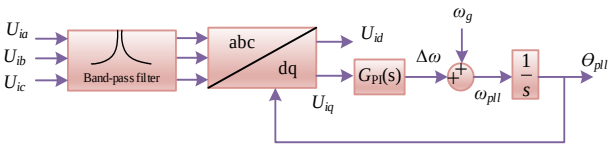

Fig. 11. BPF for restricting frequency deviation.

The expression of BPF is given by:

$$H(s) = \frac{2\xi\omega_n s}{s^2 + 2\xi\omega_n s + \omega_n^2} \tag{22}$$

where ω_n is the natural frequency and ξ the damping ratio. Bode plot is given in Fig. 12, with ω_n=100π rad/s and ξ changes from 0.05 to 0.75. It is shown that BPF only passes through the fundamental frequency and with negligible phase influence. Its damping ability for other frequency components is determined by ξ, and small ξ means large damping ability. For the system with big current reference and/or SCC, the permitted stability range for frequency deviation is small, thus smaller ξ is required to ensure system stability.

For the unstable case in Fig. 10(*b*), the simulation results are shown in Fig. 13 after applying different stability improvement methods, where applying BPF, reducing current reference, and optimizing PI parameters are respectively shown by the red-solid, blue-dotted, and black-dashed lines. It is seen that all methods can improve system stability and BPF outperforms the other two methods. The advantages and disadvantages of them are shown in Table 2 in appendix.

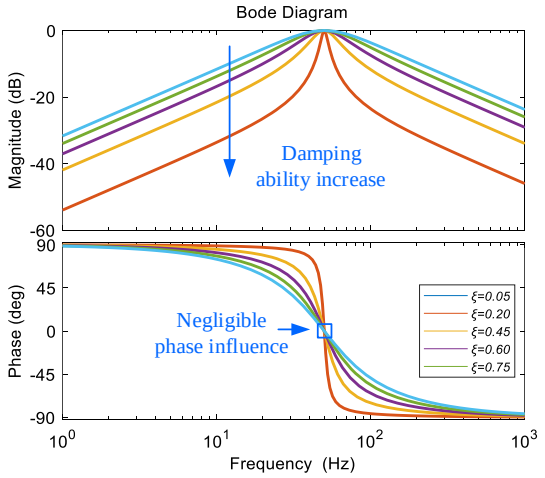

Fig. 12. Bode diagrams of BPF with different ξ.

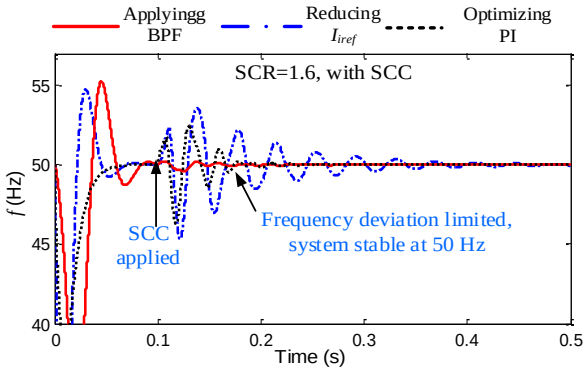

Fig. 13. Different methods to improve system stability.

4. Simulation and experimental verification

In order to verify the correctness of the stability analysis and the effectiveness of the stability improvement methods, a three-phase 500 kW inverter system and a small laboratory-scale real system were respectively built in MATLAB/Simulink with the parameters in Table 1 and our laboratory with the parameter in Table 3. The simulation and experimental results are given in this section, which are consistence with the theoretical analysis.

4.1 Simulations

In the simulations, the grid inductor was 0.4 mH which corresponding to SCR=1.16. In order to verify the instability caused by SCC and the effectiveness of the proposed stability improvement methods, SCC was firstly implemented in the normal operation system. Then, for the unstable circumstance caused by SCC, the stability improvement methods were applied such as reducing inverter current reference, adjusting PI parameters and utilizing band-pass filter. The implementation of SCC and the stability improvement methods was realized by the controllable switches. A step control signal was adopted to control the switches. Before 0.5 s, switches were controlled to connect with the original grid inductor and control parts (e.g. initial current reference, PI controller, etc.). At 0.5 s, switches were controlled to switch to the circuit with SCC, optimized PI, and band-pass filter.

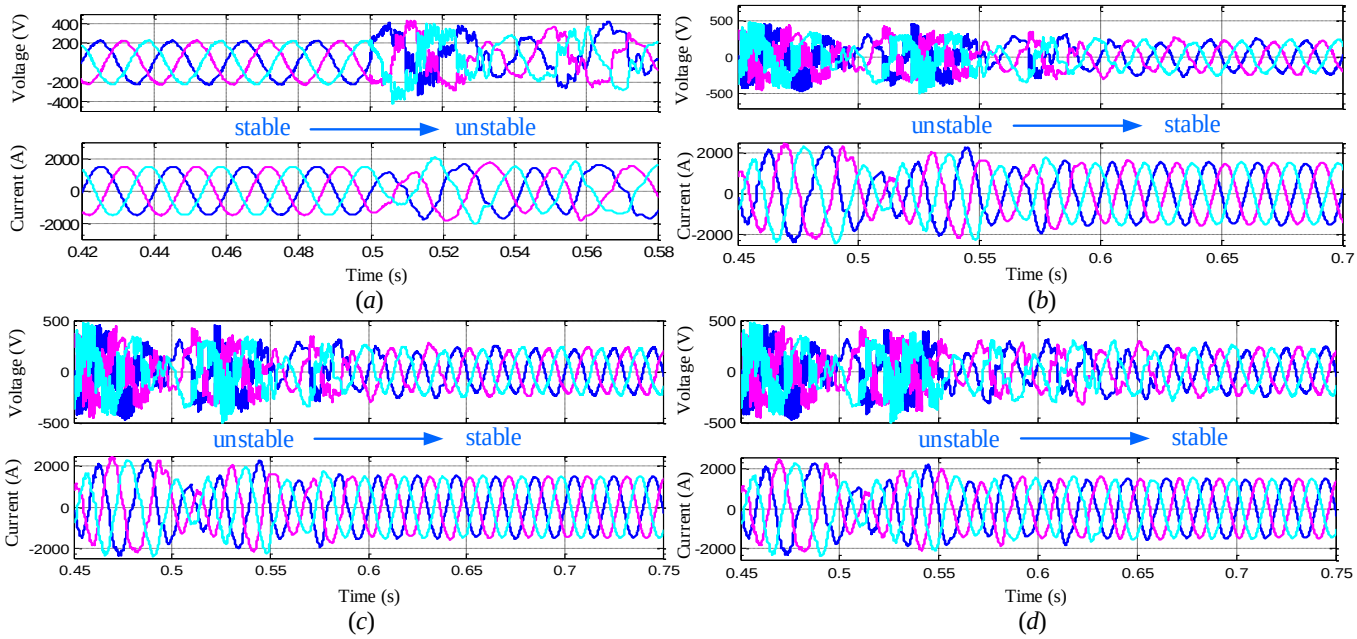

Fig. 14. Simulation results of the detailed grid-connected inverter system with SCR=1.16. (*a*): Applying SCC at 0.5 s. (*b*): Reducing current reference at 0.5 s. (*c*): Applying BPF at 0.5 s. (*d*): Optimizing PI parameters at 0.5 s.

The simulation results of the detailed inverter system are shown in Fig.14. First, the instability caused by SCC is shown in Fig. 14(*a*), where SCC was implemented at 0.5 s for the system with SCR=1.16. The resonance phenomenon of currents and voltages is due to the inverter modulation restriction (the dc side voltage cannot support the inverter side voltage when system works at the low frequency point under a large equivalent grid impedance caused by SCC). For the unstable SCC system, In Fig. 14(*b*), the current reference was reduced from 1512 A to 1000 A. It shows that reducing current reference effectively stabilizes system by expanding system stability range, which proves the theory that system instability is caused by the reduction of system stability rang shown in Fig. 7. As the reduction of current reference affects system output power in practice, two different stability improvement methods were then utilized to solve the instability problem through the switches controlled by step signal. The stabilizing process are respectively shown in Fig. 14(*c*) and Fig. 14(*d*). In Fig. 14(*c*), the band-pass filter was switched into system at 0.5 s. In Fig. 14(*d*), the original PI controller (K_P=0.7, K_I=78) was replaced by a new PI controller (K_P=0.5, K_I=5) at 0.5 s. It is shown that the original resonance system becomes stable again after applying the stability improvement methods. In addition, by the simulation waveforms, it is observed that modifying PI parameters causes system a long adjusting time than using a band-pass filter.

4.2 Experiments

Given the limits of laboratory tests, the original 500 kW inverter system was substituted with an equivalent small laboratory-scale three-phase grid-connected inverter system as shown in Fig. 15. The inverter control loop was implemented in RT-LAB real time controller. The dc side voltage was provided by the DC Sources LAB/SMS. The grid voltage was provided by a three phase step-down transformer. In the original design, the inverter working current was 2 A, and the PI controller parameters inside PLL were: K_P=0.7, K_I=78.

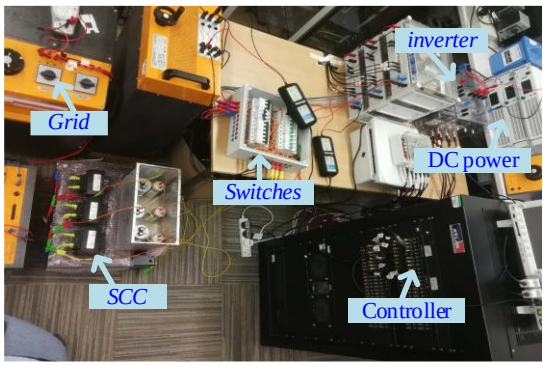

Fig. 15 Experimental system

In the experimental system, the grid impedance with and without SCC was connected with inverter by switches. By operating the switches, series capacitors were connected into system to verify the instability caused by SCC. When system with SCC, the implementation of the stability improvement methods were realized in RT-LAB. The current reference value (I_{ref}) and PI parameters (K_P, K_I) and a defined step control signal (controlling the switch in of band-pass filter) were selected as the variables in RT-LAB interface panel. Relatively control strategies were changed on line by changing the values of these variables directly in the interface panel.

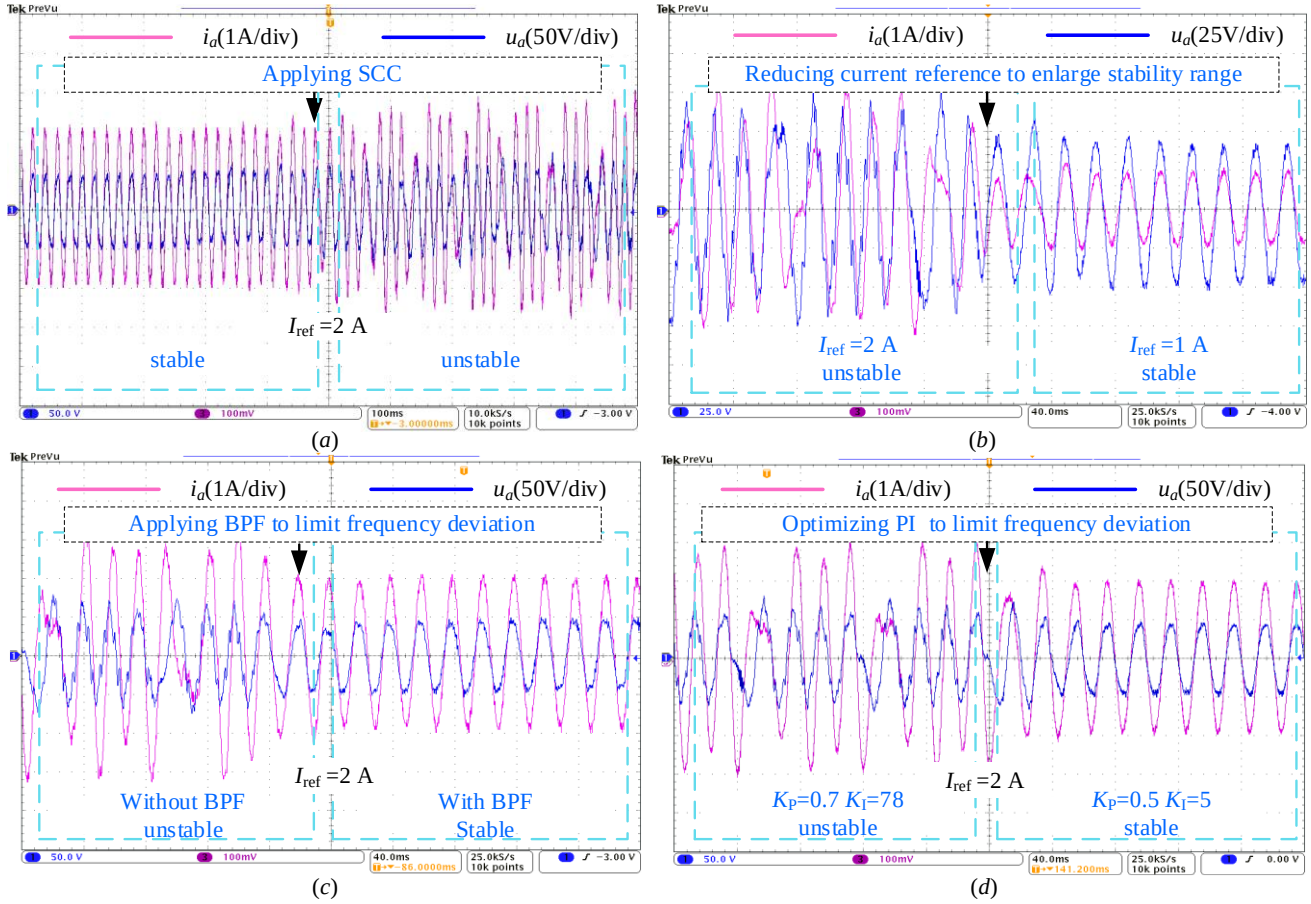

Fig. 16. Experimental results of inverter output currents and voltages of phase a. (*a*): Stable to unstable case when SCC implemented. (*b*) Reducing current reference. (*c*) Applying BPF. (*d*): Optimizing PI parameters.

The experimental results are shown in Fig. 16. Fig. 16(*a*) shows that system become resonance after applying SCC, which verifies that SCC deteriorates system stability. For the instability circumstance, Fig. 16(*b*) shows that decreasing the current reference can effectively stabilize the unstable system by broadening system stability range. In order to verify the proposed stability improvement methods, optimizing PI parameters and implementing a band-pass filter were respectively adopted for the instability case and the results are shown in Fig. 16(*c*) and Fig. 16(*d*). It shows that two methods effectively improve system stability. Therefore, the experimental results provide good support for the theoretical analysis.

5. Conclusion

SCC is commonly used for reactive power compensation and is necessary in extremely weak power grid, nevertheless, it is found out that it affects the control stability of inverters in renewable power system. The mechanism of instability and solutions for improving stability are investigated in this paper. When the system SCR is low, SCC is prone to causing system instability. The main cause of the instability is the large frequency deviation. Under a significant frequency deviation, system deviates from its fundamental frequency to another equilibrium point that is determined by inverter current control loop. To improve system stability at the fundamental frequency, methods for reducing frequency deviation by tuning PI parameters and building a BPF in front of the PLL are proposed. The results of the paper can be used to guide the stability analysis of inverters connected to a series-compensated transmission line, and are important for the utilization of renewable energy.

Appendix

Table 1 Parameters of simulation inverter

Symbol	Description	Value
U_{dc}	DC voltage	700 V
f	Fundamental frequency	50 Hz
f_s	Switching frequency	5 kHz
L_1	Inverter side filter inductor	0.2 mH
L_2	Grid side filter inductor	0.05 mH
C	Filter capacitor	220 μF
ω_0	Resonance frequency of PR controller	3.14 rad/s
k_p	Proportional term of PR controller	0.456
k_r	Resonance term of PR controller	226.076
ω_c	Bandwidth frequency of PR controller	3.14 rad/s
k_c	Active damping coefficient	0.9
U_g	Grid voltage (line-line RMS)	270 V

Table 2 Comparison of stability improvement methods

Methods	Advantages	Disadvantages
Reducing current reference	Fast, Reliable, Suitable for static stability	Power loss, Difficult to calculate the proper current
Modifying PI controller	Without additional control	Affecting system dynamic performance
Band-pass filter	Simple to realize, better performance	Needing additional filter

Table 3 Parameters of experimental inverter

Symbol	Description	Value
U_{dc}	DC voltage	100 V
f	Fundamental frequency	50 Hz
f_s	Switching frequency	10 kHz
L_1	Inverter side filter inductor	4 mH
L_2	Grid side filter inductor	2 mH
C	Filter capacitor	25 μF
ω_0	Resonance frequency of PR controller	3.14 rad/s
k_p	Proportional term of PR controller	16
k_r	Resonance term of PR controller	2000
ω_c	Bandwidth frequency of PR controller	3.14 rad/s
k_c	Active damping coefficient	25
U_g	Grid voltage (line-line RMS)	30 V

Conflict of interest statement

On behalf of all authors, the corresponding author states that there is no conflict of interest.

References

[1] S. Golestan, J. M. Guerrero, and J. C. Vasquez, "Modeling and stability assessment of single-phase grid synchronization techniques: linear time-periodic versus linear time-invariant frameworks," *IEEE Transactions on Power Electronics*, vol. 34, no. 01, pp. 20-27, 2019.

[2] J. Sun, "Impedance-based stability criterion for grid-connected inverters," *IEEE Transactions on Power Electronics*, vol. 26, no. 11, pp. 3075-3078, 2011.

[3] K. Liu, W. Cao, S. Wang, *et al*, "Admittance Modeling, Analysis, and Reshaping of Harmonic Control Loop for Multi-paralleled SAPFs System," *IEEE Transactions on Industrial Informatics*, 2021, 17(1): 280-289.

[4] Q. Peng, Q. Jiang, and Y. Yang, *et al*, "On the Stability of Power Electronics-Dominated Systems: Challenges and Potential Solutions," *IEEE Transactions on Industry Applications*, vol. 55, no. 6, pp. 7657-7670, 2019.

[5] J. G. Wang, J. D. Yan and L. Jiang *et al*, "Delay-dependent stability of single-loop controlled grid-connected inverters with LCL filters," *IEEE Transactions on Power Electronics*, vol. 31, no. 01, pp. 743-757, 2016.

[6] Y. Jin, T. Fang, and K. Yao, "An improved time-delay compensation scheme for enhancing control performance of digitally controlled grid-connected inverter," 2019 *IEEE Energy Conversion Congress and Exposition (ECCE)*, Baltimore, MD, USA, 2019, pp. 2772-2776.

[7] Y. Li, Y. Gu, Y. Zhu, *et al*, "Impedance Circuit Model of Grid-Forming Inverter: Visualizing Control Algorithms as Circuit Elements," *IEEE Transactions on Power Electronics*, vol. 36, no. 3, pp. 3377-3395, 2021

[8] W. Du, F. Tuffner, and K. P. Schneider, *et al*, "Modeling of Grid-Forming and Grid-Following Inverters for Dynamic Simulation of Large-Scale Distribution Systems," *IEEE Transactions on Power Delivery*, vol. 36, no. 4, pp. 2035-2045, 2021.

[9] Q. Zhang, L. Zhou, and M. Mao, *et al*, "Power quality and stability analysis of large-scale grid-connected photovoltaic system considering non-linear effects," *IET Power Electronics*, vol. 11, no. 11, pp. 1739-1747, 2018.

[10] Y. Ren, X. Wang, and L. Chen, *et al*, "A Strictly Sufficient Stability Criterion for Grid-Connected Converters Based on Impedance Models and Gershgorin's Theorem," *IEEE Transactions on Power Delivery*, vol. 35, no. 3, pp. 1606-1609, 2020.

[11] L. Zhou, W. Wu, and Y. Chen, *et al*, "Virtual Positive-Damping Reshaped Impedance Stability Control Method for the Offshore MVDC System," *IEEE Transactions on Power Electronics*, vol. 34, no. 5, pp. 4951-4966, 2019.

[12] H. Kim, H. Jung, and S. Sul, "Discrete-Time Voltage Controller for Voltage Source Converters With LC Filter Based on State-Space Models," *IEEE Transactions on Industry Applications*, vol. 55, no. 1, pp. 529-540, 2019.

[13] S. G. Vennelaganti and N. R. Chaudhuri, "Stability Criterion for Inertial and Primary Frequency Droop Control in MTDC Grids With Implications on Ratio-Based Frequency Support," *IEEE Transactions on Power Systems*, vol. 35, no. 5, pp. 3541-3551, 2020.

[14] F. Al Hasnain, A. Sahami and S. Kamalasadan, "An Online Wide-Area Direct Coordinated Control Architecture for Power Grid Transient Stability Enhancement Based on Subspace Identification," *IEEE Transactions on Industry Applications*, vol. 57, no. 3, pp. 2896-2907, 2021.

[15] C. Zhang, M. Molinas, and A. Rygg, *et al*, "Impedance-Based Analysis of Interconnected Power Electronics Systems: Impedance Network Modeling and Comparative Studies of Stability Criteria," *IEEE Journal of Emerging and Selected Topics in Power Electronics*, vol. 8, no. 3, pp. 2520-2533, 2020.

[16] E. Buraimoh and I. E. Davidson, "Simplified LCL Filter State Space Modeling and Small Signal Stability Analysis of Inverter Based Microgrid," *2021 IEEE PES/IAS PowerAfrica*, Nairobi, Kenya, 2021, pp. 1-5.

[17] J. Hu, Q. Hu, and B. Wang et al, "Small signal instability of PLL-synchronized Type-4 wind turbines connected to high-impedance AC grid during LVRT," *IEEE Transactions on Energy Conversion*, vol. 31, no. 4, pp. 1676-1687, 2016.

[18] X. Zhang, D. Xia, and Z. Fu *et al*, "An improved feedforward control method considering PLL dynamics to improve weak grid stability of grid-connected inverters," *IEEE Transactions on Industry Applications*, vol. 54, no. 5, pp. 5143-5151, 2018.

[19] L. Huang, H. Xin, and Z. Li, "Grid-synchronization stability analysis and loop shaping for PLL-based power converters with different reactive power control," *IEEE Transactions on Smart Grid*, vol. 11, no. 01, pp. 501-516, 2020.

[20] X. He, H. Geng and S. Ma, "Transient stability analysis of grid-tied converters considering PLL's nonlinearity," *CPSS Transactions on Power Electronics and Applications*, vol. 4, no. 1, pp. 40-49, 2019.

[21] Q. Zhang, M. Mao, and G. Ke *et al*, "Stability problems of PV inverter in weak grid: a review," *IET Power Electronics*, 2020, 13(11): 2165-2174.

[22] S. Ghosh, Y. J. Isbeih, and R. Bhattarai *et al*, "A dynamic coordination control architecture for reactive power capability enhancement of the DFIG-Based wind power generation," *IEEE Transactions on Power Systems*, vol. 35, no. 4, pp. 3051-3064, 2020.

[23] P. Li, L. Xiong, and Z. Wang *et al*, "Fractional-order sliding mode control for damping of subsynchronous control interaction in DFIG-based wind farms," *Wind Energy*, vol. 5, no. 3, pp. 749-762, 2020.

[24] Y. Xu, S. Zhao, "Mitigation of Subsynchronous resonance in series-compensated DFIG wind farm using active disturbance rejection control," *IEEE Access*, vol. 7, pp. 68812-68822, 2019.

[25] J. Shair, X. Xie, and L. wang *et al*. "Overview of emerging subsynchronous oscillations in practical wind power systems" *Renewable and Sustainable Energy Reviews*, vol. 99, pp. 159-168, 2019

[26] N. Cao, Z. Song, and K. Chong *et al*, "Research on SSCI caused of doubly fed wind power generation via fixed series compensated transmission," *2017 Chinese Automation Congress (CAC)*, Jinan, 2017, pp. 3711-3717.

[27] S. Ma, H. Geng, and L. Liu et al, "Grid-synchronization stability improvement of large scale wind farm during severe grid fault," *IEEE Transactions on Power Systems*, vol. 33, no. 1, pp. 216-226, 2018.

[28] X. F. Wang, L. Harnefors, and F. Blaabjerg, "Unified impedance model of grid-connected voltage-source converters", *IEEE Transactions Power Electron.*, vol. 33, no. 2, pp. 1775-1787, 2018.

[29] Q. Hu, L. Fu, and F. Ma *et al*, "Large signal synchronizing instability of PLL-based VSC connected to weak AC grid," *IEEE Transactions on Power Systems*, vol. 34, no. 4, pp. 3220-3229, 2019.

[30] J. Zhao, M. Huang, and H. Yan, *et al*, "Nonlinear and Transient Stability Analysis of Phase-Locked Loops in Grid-Connected Converters," *IEEE Transactions on Power Electronics*, vol. 36, no. 1, pp. 1018-1029, 2021.

[31] D. Dong, B. Wen, D. Boroyevich, et al, "Analysis of Phase-Locked Loop Low-Frequency Stability in Three-Phase Grid-Connected Power

Converters Considering Impedance Interactions," *IEEE Transactions on Industrial Electronics*, vol. 62, no. 1, pp. 310-321, Jan. 2015.
[32] P. Rodríguez, J. Pou, J. Bogas, et al, "Decoupled Double Synchronous Reference Frame PLL for Power Converters Control," *IEEE Transactions on Power Electronics*, vol. 22, no. 2, pp. 584-592, 2007.

Qianjin Zhang received his B.S. degree in electrical engineering from Shandong Agricultural University, Tai'an, China, in 2015. He received his Ph.D. degree in power electronics from Chongqing university, Chongqing, China, in 2020. He was a visiting student in the University of Exeter, Penryn, UK, from May 2018 to May 2019. He is presently a lecture in Anhui University of Technology, Anhui, China. His research interests include PV generation, the modeling and stability analysis of power electronics system.

Jinhui Qian received his B.S. degree in electrical engineering from Changzhou Institute of Technology, Chang Zhou, China, in 2021. He is presently working towards his M.S. degree in power electronics in Anhui University of Technology, Anhui, China. His current research interests include stability analysis of grid-connected inverters.

Zhaorong Zhai received her B.S. degree in electrical engineering from Huainan Normal University, Anhui, China, in 2021. She is presently working towards his M.S. degree in power electronics in Anhui University of Technology, Anhui, China. Her current research interests include design and intelligent control of inverters.

Mohammad Abusara received his B.S. degree from Birzeit University, Palestine, in 2000 and his PhD degree from the University of Southampton, UK, in 2004, both in electrical engineering. He is currently a professor in the University of Exeter, Penryn, UK. His current research interests include grid and parallel-connected inverters, micro-grid, DC/DC converters for hybrid vehicles, and sensorless drives for high speed permanent magnet machines.

Xiaodong Liu received the Ph.D. degree in electric machines and electric apparatus from Zhejiang University, Hangzhou, China, in 1999. Since 2003, he has been a professor in Anhui University of Technology, Ma'anshan, China. His research interests include the renewable power generation, dc microgrids.

Sucheng Liu received the Ph.D. degree in electrical engineering from Chongqing University, Chongqing, China, in 2013. He has been an associate professor since 2016 in Anhui University of Technology, Ma'anshan, China. His research interests include modeling and control of dc microgrids and clusters.

Wei Fang received the Ph.D. degree in control theory and control engineering from Nanjing University of Aeronautics and Astronautics, Nanjing, China, in 2008. He is currently a professor in Anhui University of Technology, Annhui, China. His research interests include design and control of power electronics.

Hongbo Liu received her B.S., and Ph.D. degrees in Electrical Engineering from Chongqing University, Chongqing, China, in 2015, 2020, respectively. He is presently working in Qingdao Power Supply Company, Qingdao, China. His current research interests include high voltage power electronics system.